Folding flexible co-extruded all-polymer multilayer distributed feedback films to control lasing

James H. Andrews,[1,*] Michael Crescimanno,[1] Nathan J. Dawson,[1] Guilin Mao,[1] Joshua B. Petrus,[1] Kenneth D. Singer,[2,3] Eric Baer,[3] and Hyunmin Song[3]

[1] *Dept. of Physics & Astronomy, Youngstown State Univ., Youngstown, Ohio 44555, USA*
[2] *Dept. of Physics, Case Western Reserve Univ., Cleveland, Ohio 44106, USA*
[3] *Macromolecular Science and Engineering, Case Western Reserve Univ., Cleveland, Ohio 44106, USA*
[*] *jandrews@ysu.edu*

Abstract: We report on improved gain and spectral control in co-extruded all-polymer multilayer distributed feedback (DFB) lasers achieved by folding and deliberate modification of the center "defect" layer. Because DFB laser gain is greater at spectral defects inside the reflection band than at the band edges, manipulation of structural defects can be used to alter spectral defects and thereby tune the output wavelength and improve laser efficiency. By experimentally terracing the layer that becomes the center of the fold, we tuned the lasing wavelength across the reflection stop-band ($\sim$25 nm) in controllable, discrete steps. The increased density of states associated with the defect resulted in a lower lasing threshold and, typically, a 3- to 6-fold increase in lasing efficiency over non-folded samples.

OCIS codes: (140.3945) Microcavities; (160.5293) Photonic bandgap materials; (160.5470) Polymers; (140.2050) Dye lasers.

References and links

1. H. Song, K. Singer, J. Lott, Y. Wu, J.Zhou, J. Andrews, E. Baer, A. Hiltner, and C. Weder, "Continuously melt processing of all-polymer distributed feedback lasers," J. Mater. Chem. **19**, 7520–7524 (2009).
2. K. D. Singer, T. Kazmierczak, J. Lott, H. Song, Y. Wu, J. Andrews, E. Baer, A. Hiltner, and C. Weder, "Melt-processed all-polymer distributed Bragg reflector laser," Opt. Express **16**, 10358–10363 (2008).
3. T. Kazmierczak, H. Song, A. Hiltner, and E. Baer, "Polymeric one-dimensional photonic crystals by continuous coextrusion," Macromol. Rapid Commun. **28**, 2210–2216 (2007).
4. T. Komikado, S. Yoshida, and S. Umegaki, "Surface-emitting distributed-feedback dye laser of a polymer multilayer fabricated by spin coating," Appl. Phys. Lett. **89**, 061123 (2006).
5. H. Takeuchi, K. Natsume, S. Suzuki, and H. Sakata, "Microcavity distributed-beedback laser using dye-doped polymeric thin films," Electron. Lett. **43**, 30–32 (2007).
6. C. Kallinger, M. Hilmer, A. Haugeneder, M. Perner, W. Spirkl, U. Lemmer, J. Feldmann, U. Scherf, K. Mullen, A. Gombert, and V. Wittwer, "A flexible conjugated polymer laser," Adv. Mater. **10**, 920–923 (1998).
7. O. Garcia, R. Sastre, I. Garcia-Moreno, V. Martin, and A. Costela, "New laser hybrid materials based on POSS copolymers," J. Phys. Chem. C **112**, 14710–14713 (2008).
8. J. Zhou, K. D. Singer, J. Lott, H. Song, Y. Wu, J. Andrews, E. Baer, A. Hiltner, and C. Weder, "All-polymer distributed feedback and distributed Bragg-reflector lasers produced by roll-to-roll layer-multiplying co-extrusion," Nonlinear Opt., Quantum Opt. **41**, 59–71 (2010).
9. G. Mao, J. Andrews, M. Crescimanno, K. D. Singer, E. Baer, A. Hiltner, H. Song, and B. Shakya, "Co-extruded mechanically tunable multilayer elastomer laser," Opt. Mater. Express **1**, 108–114 (2011).

#167148 - $15.00 USD Received 20 Apr 2012; revised 7 Jun 2012; accepted 7 Jun 2012; published 26 Jun 2012

10. E. Yablonovich, T. J. Gmitter, R. D. Meade, A. M. Rappe, K. D. Brommer, and J. D. Joannopoulos, "Donor and acceptor modes in photonic band structure," Phys. Rev. Lett. **67**, 3380–3383 (1991).
11. E. Yablonovitch, "Inhibited spontaneous emission in solid-state physics and electronics," Phys. Rev. Lett. **58**, 2059–2062 (1987).
12. H. Yoshida, C. H. Lee, Y. Miura, A. Fujii, and M. Ozaki, "Optical tuning and switching of photonic defect modes in cholesteric liquid crystals," Appl. Phys. Lett. **90**, 071107 (2007).
13. J. Schmidtke, W. Stille, and H. Finkelmann, "Defect mode emission of a dye doped cholesteric polymer network," Phys. Rev. Lett. **90**, 083902 (2003).
14. J. P. Dowling, M. Scalora, M. J. Bloemer, and C. M. Dowden, "The photonic band edge laser: a new approach to gain enhancement," J. Appl. Phys. **75**, 1896–1899 (1994).
15. S. Nojima, "Enhancement of optical gain in two dimensional photonic crystals with active lattice points," Jpn. J. Appl. Phys., Part 2 **37**, L565–L567 (1998).
16. J. Yoon, W. Lee, J.-M. Caruge, M. Bawendi, E. L. Thomas, S. Kooi, and P. N. Prasad, "Defect-mode mirrorless lasing in dye-doped organic/inorganic hybrid one-dimensional photonic crystal," Appl. Phys. Lett. **88**, 091102 (2006).
17. S. M. Jeong, N. Y. Ha, Y. Takanishi, K. Ishikawa, H. Takezoe, S. Nishimura, and G. Suzaki, "Defect mode lasing from a double-layered dye-doped polymeric cholesteric liquid crystal films with a thin rubbed defect layer," Appl. Phys. Lett. **90**, 261108 (2007).
18. V. Milner and A. Z. Genack, "Photon localization laser: Low-threshold lasing in a random amplifying layered medium via wave localization," Phys. Rev. Lett. **94**, 073901 (2005).
19. P. Yeh, *Optical Waves in Layered Media* (Wiley Interscience, 2005).
20. L. A. A. Pettersson, L. S. Roman and O. Inganäs, "Modeling photocurrent action spectra of photovoltaic devices based on organic thin films," J. Appl. Phys. **86**, 487–496 (1999).
21. J. D. Joannapolous, S. G. Johnson, J. N. Winn, and R. D. Meade, *Photonic Crystals; Molding the Flow of Light* (Princeton, 2008) p. 147.
22. N. Le Thomas, V. Zabelin, and R. Houdré, "Influence of residual disorder on the anticrossing of Bloch modes probed in *k* space," Phys. Rev. B **78**, 125301 (2008).
23. I. Rendina, F. Coppinger, B. Jalali, C. Lam, and E. Yablanovich, "Coupled Cavity Distributed-Resonance Photodetectors," SPIE Photonics West '98 **3278**, Integrated Optical Devices II, San Jose, Ca, Jan. 28–30 (1998).

1. Introduction and background

Recent advances in all-polymer, roll-to-roll processable lasers [1,2] (process in [3]) and in polymer lasers in general [4–7] provide significant new opportunities for enhancing nonlinear optical processes through the controlled design of wave dispersion in a one-dimensional multilayer "photonic crystal" (PhC) structure. These advances include lasing in multiple configurations, such as Distributed Bragg Reflector (DBR) lasers (multilayer Bragg reflectors surrounding a center gain layer), Distributed Feedback (DFB) lasers (gain medium layered throughout the multilayer structure), various gain media [8], multi-wavelength lasing and broadly-tunable, reversible, mechanical tuning [9]. The engineering and economic promise of the all-polymer, roll-to-roll processable PhC laser is a result of the broad range of inexpensive polymers, dyes, and other active media from which a diverse and controlled set of structures with gain across various wavelength ranges can be fashioned. The compact physical length of these flexible lasers (a few tens of microns at their thickest) has important implications for tunability, intercavity dispersion control and applications. Most importantly for this study, the mechanical properties of these multilayers enable simple post-processing, such as folding and center layer modification, to create additional phase-shifts.

Folding explicitly breaks the discrete translation symmetry of the stack, introducing, as is well known [10], an "impurity band" in the center of the reflection band. The position of the band is a function of the phase accumulation ("phase slip" [11]) associated with transport through that defect. As a class of metamaterials, these roll-to-roll processable PhC's are quite distinct, however, from semiconductor DFB lasers and liquid crystal (LC)-based efforts. The latter includes many promising advances such as discrete spectral tuning and switching (discrete- or step-tuning) of a defect [12, 13] that could serve as a dispersive element in a cholesteric LC (CLC).

#167148 - $15.00 USD Received 20 Apr 2012; revised 7 Jun 2012; accepted 7 Jun 2012; published 26 Jun 2012

Unlike in conventional DFB lasers, in the folded PhC DFB laser described here, lasing occurs predominantly at the reflection band defect, a phenomenon that we take advantage of in two ways. First, by folding a 64-layer all-polymer DFB multilayer laser film made using our previously reported coextrusion method [1], we have created 128-layer DFB laser films with a thickened central region that leads to a narrow spectral defect (i.e., a local transmission peak) in the reflection band at which we observe low-threshold, high-efficiency lasing. The lasing spectra and the threshold and optical conversion efficiency of these folded films were compared to their counterpart, a 128-layer DFB laser film made by coherent stacking of two 64-layer multilayer DFB laser films in the same orientation. The defect (folded) films show better wavelength controllability, lower lasing thresholds, and significantly higher optical efficiencies.

Second, by creating a terraced central defect layer with three different center thicknesses in a single folded film, we demonstrate lasing at three different wavelengths within the reflection band using the same extruded film. This simple terracing of a single central layer provides a way of discretely tuning the lasing wavelength and also suggests a way to continuously tune the lasing wavelength by using a wedge central defect layer, taking advantage of the broad tunability of the gain spectrum of the R6G lasing dye.

Finally, to better understand the contributions of dispersion of the defect lasing mode, we simulate, using transfer matrix techniques, the predicted gain profiles of the multilayer structures and the effects of including a linear gain medium in the different constituents and different fold configurations. These simulations are consistent with the experiment in that they qualitatively indicate significant increases in the system gain at the reflection band defects.

2. Materials and experiment

The multilayer films used in the experiments described below were fabricated using the coextrusion process reported previously [1, 3]. The experimental setup shown in Fig. 1(a) characterizes the DFB lasers. These films contain 64 alternating layers of dye-doped poly(styrene-co-acrylonitrile) with 25 wt% acrylonitrile (SAN25, refractive index=1.57) and a fluoroelastomer terpolymer of vinylidene fluoride, exafluoroproplyene, and tetrafluoroethylene (Dyneon THV 220G, refractive index=1.37), with an average bilayer periodicity of 200 nm and with rhodamine-6g (R6G) laser dye dissolved in the SAN25 layers at a nominal dye concentration of 1 wt% [1, 8]. As detailed in our earlier work, the R6G dye was dissolved in the polymer of higher refractive index layers (SAN25) for the practical reason that the R6G dye was not compatible with the THV polymer during extrusion. In fact, the THV polymer was chosen in part because it acted as a barrier layer, inhibiting dye diffusion.

Four types of samples were made and used in these experiments:

#1 Folded 64-layer DFB SAN25/THV laser film, which results in a 128-layer film with a doubled SAN25 (higher refractive index) center defect layer, $(THV/SAN25)^{32}(SAN25/THV)^{32}$, as illustrated in Fig. 1(b);

#2 Folded 64-layer DFB SAN25/THV laser film, which results in a 128-layer film with a doubled THV (lower refractive index) center defect layer, $(SAN25/THV)^{32}(THV/SAN25)^{32}$;

#3 Stacked pair of 64-layer samples (no-folding) in the same orientation to obtain a simple 128-layer laser film, $(SAN25/THV)^{64}$; and

#4 Folded 64-layer DFB SAN25/THV laser film, as in #2, but with the center THV layer etched before folding using a repeated ethanol wipe along the edge of a glass cover slip to form a terraced layer with three different thicknesses.

#167148 - $15.00 USD Received 20 Apr 2012; revised 7 Jun 2012; accepted 7 Jun 2012; published 26 Jun 2012

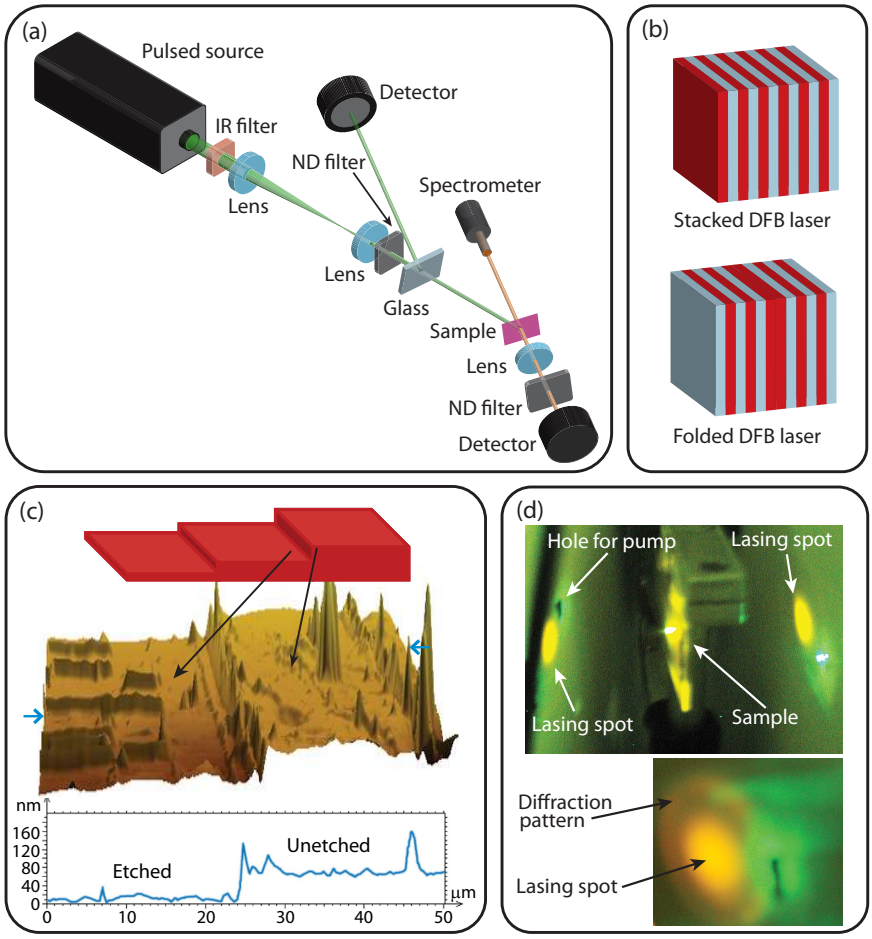

Fig. 1. (a) The experimental setup used to characterize the DFB lasers (ND = Neutral Density, IR = Infra Red), (b) illustrations of a stacked and folded SAN25/THV DFB laser film, (c) an AFM image of the first etched step (etched region at left) in the terraced and folded DFB laser with cross-section below taken at the marked location on the image, and (d) photographs of laser emission from a DFB laser folded-on-SAN25 sample type (#1) showing approximately equal lasing from both faces of the microcavity laser and a close-up image of yellow beam spot with an additional ring due to diffraction.

Thus, for sample #4, the final 128-layer defect laser film was constructed with a tiered central defect of three defect thicknesses at three different locations with etch steps of ∼60 nm. An AFM image of one of the steps is shown in Fig. 1(c). Binding of the folded surfaces was accomplished through static cling.

Layer thickness variations produced by the coextrusion process (increasing with the number of layers) were previously estimated to be about ∼18% for the 64 layer films, but are not Gaussian. These variations are discussed in [1, 3] where, for example, analysis of 59 of the 64 layers in an AFM cross-section of a different location on the film revealed average THV and SAN25 layer thicknesses of 96 nm and 105 nm, respectively. For the experiments reported here, samples were selected on the basis of reflection band uniformity (fewest and least pronounced defects, also suggesting better layer uniformity) prior to folding. The absence of significant

#167148 - $15.00 USD Received 20 Apr 2012; revised 7 Jun 2012; accepted 7 Jun 2012; published 26 Jun 2012

defects in the reflection bands of the stacked samples (#3) further evinces that our stacking method does not introduce significant air gaps between the surfaces.

The DFB films were pumped at a 20° incident angle by frequency-doubled Nd:YAG laser pulses (λ =532 nm, 10 Hz, S-polarized). We used a knife-edge technique to measure the spot size of the pump beams. In two different experimental tests reported here, the pump beam waists are 50 μm and 120 μm with 75 ns and 7 ns full-width at half-maximum pulse durations, respectively. We measured the output spectrum using a compact spectrometer (USB4000UV-VIS, Ocean Optics) and the laser powers using a fast silicon photodiode (Det110, Thorlabs) triggered by a reference beam, where both the reference and output detectors were calibrated using a pyroelectric detector (QE12LP, Gentec).

Figure 2 shows a range of typical output powers of sample types (#1) through (#3) (two of each type) as a function of the input power. The corresponding transmission (black line) and emission (red line) spectra are shown above and below Figs. 2(a) and 2(b), where the arrows indicate the spectra graphs corresponding to each efficiency curve. The transmission spectra are similar except that each folded defect laser film shows a spectral defect inside the reflection band. Additional features in the transmission spectra are believed to be the result of layer thickness variations. (The region spanning from 570nm to 610nm is the reflection band, whereas the absorption band of the R6G laser dye ends around 550 nm.)

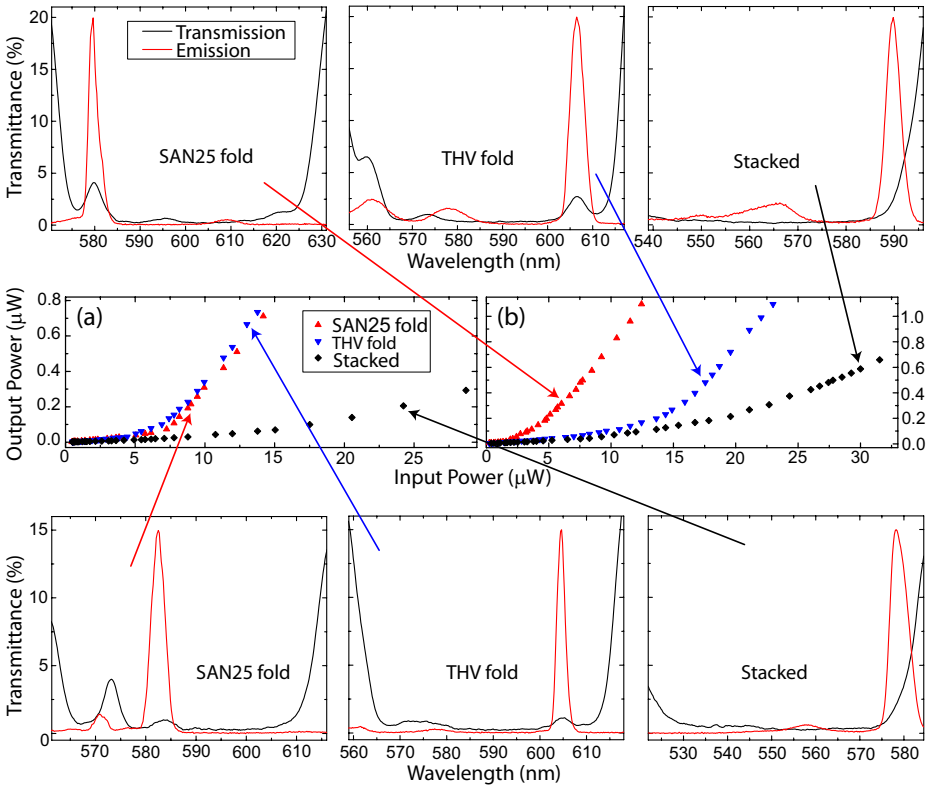

Fig. 2. (a) Comparative conversion efficiency curves of sample types (#1)-(#3) with their corresponding transmission and emission spectra pumped by the source with a 75 ns pulse duration. (b) A second set of comparative conversion efficiency curves for the same sample types but from a different section of the extruded multilayer film and a different pump laser with a 7 ns pulse duration and a larger spot size.

#167148 - $15.00 USD Received 20 Apr 2012; revised 7 Jun 2012; accepted 7 Jun 2012; published 26 Jun 2012

As the pump power incident on the films was increased, the transition from amplified spontaneous emission (ASE) to lasing was evident from the beaming of the output normal to the surface (Fig. 1(d) and the dramatic increase in output efficiency over a narrowed spectral range; see also [1, 8]). (Note that ASE and lasing appeared at wavelengths well beyond the fluorescence maximum at 552 nm.) The roughness of the surfaces and layer thickness variations across the area pumped led to a multiple spatial modes, but we were unable to resolve the individual modes with the broadband spectrometer used as its resolution was limited by pixel-to-pixel relative intensity.

Most interesting for this study are the different output wavelengths, efficiencies, and thresholds, which depend upon the type of sample #1-#3. The lasing wavelength for each stacked film (#3) corresponds approximately to the long wavelength (low energy) reflection band edge, as expected. With the folded samples, #1 and #2, however, the lasing wavelength closely corresponds to the reflection band defects. Two different experimental sets are shown in order to illustrate the range of data observed with comparable films for experiments actually performed several months apart. (The efficiencies, thresholds, and output spectra showed no special dependence upon which pump laser was used, however.) These data show similar lasing slope efficiencies for the folded structures, but exhibit lasing threshold dependence on finer details of the films' transmission and emission spectra. The differences in ASE and lasing thresholds appear to be attributable to variations in layer thickness that lead to unintended defect modes that compete for gain at low pump levels. This effect can be seen, for example, in the lasing spectrum of sample type #1 (folded-on-SAN25) in Fig. 2(a) (bottom left) at around 573 nm and also in Fig. 3 at around 578 nm, leading to an additional (weak) lasing line.

The optical efficiency curves in both Fig. 2(a) and 2(b) indicate comparable lasing slope efficiencies for both folding schemes (#1, #2) that are three to six times higher than for the stacked counterpart laser film sample (#3) tested under identical experimental conditions. The lasing slope efficiencies of the #1 (folded-on-SAN25), #2 (folded-on-THV), and #3 (stacked) films are found to be about 8%-10%, 8%-10%, and 1.3%-3.0%, respectively; in the ASE region, the slope efficiencies of films #1, #2, and #3 are approximately 0.8%-1.3%, 0.7%-0.9%, and 0.3%-0.5%, respectively. We give the ranges of the observed data rather than the slope uncertainties because the differences between locations were much larger than the uncertainties in the calculated slopes for each data set. To measure the efficiencies, the reflection of the pump beam at the interface of the film surface and air was subtracted from the incident power. The output power was only measured from one side of the film, and so the total output power was multiplied by a factor of 2, assuming equal output intensities from each face (see Fig. 1(d)).

The measured threshold values are also typically much lower for folded sample types #1 and #2 though additional defects due to random variations of the layer thicknesses throughout the multilayered material compete, thereby increasing the threshold. We give thresholds in terms of the intensity per pulse as opposed to fluence because the fluorescent lifetime at our concentration of R6G (nominal concentration of 0.23 M) is in the 10^{-10} s timescale, which is an order of magnitude less than the shortest pump pulse duration used. The optimum lasing threshold intensities without additional defect competition for films #1, #2, and #3, all pumped with a Gaussian beam, are estimated at 110 kW/cm^2, 110 kW/cm^2, and 240 kW/cm^2, respectively, though thresholds for the THV-fold lasers were often lower than for the SAN25-fold lasers by up to a factor of almost two.

Next, we studied sample #4, which was folded on the THV side after terracing the thickness of that outer layer as previously described to create a central terraced defect layer. Figure 3(a) shows the transmission curves of this terraced and folded sample at three different center layer thicknesses, which shows the shift of the spectral defect across the entire reflection band. All three curves show two spectral defect peaks inside the reflection band. The first defect peak

#167148 - $15.00 USD Received 20 Apr 2012; revised 7 Jun 2012; accepted 7 Jun 2012; published 26 Jun 2012

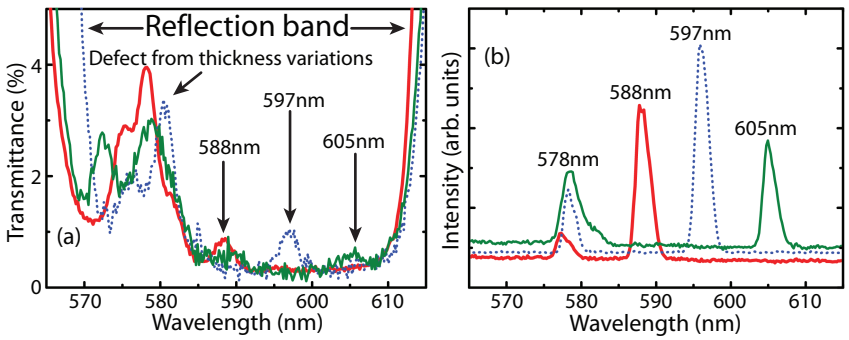

Fig. 3. (a) Transmission curve of 128-layer folded terraced-defect laser film. (b) Laser spectra of the 128-layer folded terraced-defect laser film at three different center thicknesses.

around 578nm is due to the layer thickness variation within the film created during the extrusion process [1]. The matching of the three transmission curves at this defect indicates that the laser film is uniform laterally over the size of our sample and that the thickness variation at the center of the fold is the primary distinguishing characteristic between regions. The longer wavelength spectral defect in each curve corresponds to the spectral defect created by the terraced center thickness of the folded structure.

At each center thickness value, the laser initially lased at two wavelengths simultaneously. At the different center thicknesses, only the longer lasing wavelength changes, corresponding to the position of the spectral defects in the curves as seen in comparing the laser spectrum in Fig. 3(b) with the transmission spectra in Fig. 3(a). Well above threshold, however, we found that lasing output at the spectral location associated with the terraced fold defect was significantly greater than that seen at the inherent shorter wavelength reflection band defect. This technique thus demonstrates a way of controlling the lasing wavelength by changing the thickness of the central defect layer even in the presence of some layer thickness variation throughout the stack.

3. Discussion and numerical simulations

It is well known that the slowing of the group velocity (increased density of states) at the band edge and at band defects typically implies that the lasing threshold will be lower at these spectral locations in PhC lasers [14, 15], and reflection band defect mode lasing appears to be a promising archetype for low-threshold lasing in 1-d PhCs [16, 17]. Ref. 16, for example, which describes a PhC with a very thick defect layer, relates the lasing enhancement at the defect state to an increase in the local density of states or, equivalently, to a reduction of the group velocity through the stack at the defect wavelength. Similarly, [18] found that a randomly amplified layered lasing medium can lead to significantly lower lasing thresholds due to long-lived localized modes that overlap spatially with the localized gain medium.

To better understand the effects of microstructure on the lasing thresholds and gain, we use standard transfer matrix theory to model the effects of the multilayer geometries [19]. In Fig. 4(a), we graph the transmission of a perfect THV/SAN25 multilayer with a thickness of 100 nm per layer, (a) not folded and simply folded and (b) where we change the thickness of the central (fold) THV layer. (The features are spectrally averaged to more closely match our detection and the lateral variation across the probing beam.) As can be seen, the location of the reflection band defect can be moved by controlling the thickness of the center layer, so as to appear at different positions inside the reflection band, as was seen experimentally in Fig. 3(a). We believe that the difference in sharpness of the defect is due to the lateral as well as longitudinal layer

#167148 - $15.00 USD Received 20 Apr 2012; revised 7 Jun 2012; accepted 7 Jun 2012; published 26 Jun 2012

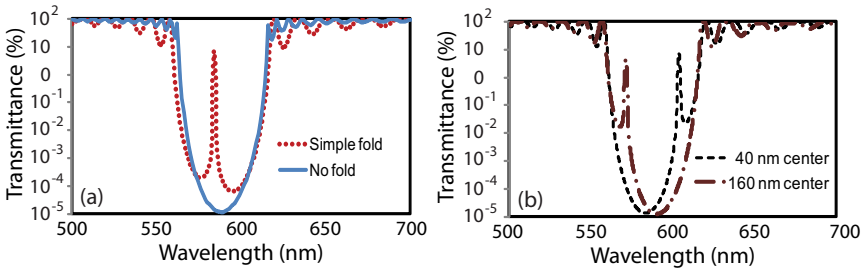

Fig. 4. (a) Transmission of simple multilayer, $(\mathrm{THV/SAN25})^{64}$ (solid blue trace) and transmission of a folded multilayer, $(\mathrm{SAN25/THV})^{32}(\mathrm{THV/SAN25})^{32}$ (dotted red trace), both with 100 nm per layer; (b) transmission of the folded 128-layer film with a terraced central (THV) defect layer.

thickness variations and the finite spectral width detection of our broadband spectrometer. As the center layer is thinned, the spectral defect moves to shorter wavelengths until the quarter-wave thickness is reached and the reflection band defect disappears. As the center layer is thinned still further, the spectral defect reappears near the long wavelength band edge and, from there, shifts again towards shorter wavelengths as the center layer is thinned further.

For further comparison, we also calculated the peak electric field energy density for idealized 32, 64, and 128 layer folded and stacked structures in transmission using the method described in [20]. In each case, we found that (1) the folded structure produces a peak internal field energy density at the spectral defect that greatly exceeds the internal field energy density at either band edge of a simple stacked structure with the same number of layers, but that (2) the peak energy density appears over a more localized region near the center of the fold. Increasing the number of bilayers further increases and localizes the peak internal electric field energy density in the folded structure relative to the equivalent stacked structure.

We now describe the effects of (linear) gain/absorption in one of the materials making up the multilayer by way of adding a (spectrally flat) negative imaginary contribution to the refractive index and plotting the resulting increased output (gain) in Fig. 5. Generally, the reflection band edges are the first to exhibit large gain, consistent with the well known scaling of gain at a reflection band edge (expected to go as $1/v_g$ near the band edge (see [21]), and v_g is expected to vanish as a power law in an infinite perfect system. In a disordered system, however, v_g is expected to vanish logarithmically with the disorder parameter–which scales as the inverse of the number of layers, $1/N$, for a finite system [22]). Whether the lasing threshold is first found at the high-energy or the low-energy edge of the reflection band depends upon whether the gain medium is in the lower refractive index or higher refractive index constituent, respectively. Although band edge lasing is predicted for the perfectly regular multilayer, this is not where lasing typically appears in experiments where the layer thicknesses are not uniform or where a phase slip defect appears in the stack. (In earlier work, we saw that random thickness variations resulted in lasing at a reflection band defect [1], even without intentional folding.) The presence of disorder decreases gain at the band edge, indicating that the corresponding lasing threshold there has been consequently increased.

Figure 5, in which A (B) is the higher (lower) refractive index material, shows that the optimal structure for the defect DFB laser is to have the gain in the low index B material (here THV) and at the center of the fold (the so-called "acceptor" geometry; see [10]). In the two panels in Fig. 5, all for hypothetical structures $(AB)^{32}(BA)^{32}$ and $(BA)^{32}(AB)^{32}$, the same absorption/gain parameter is in entirely one species or the other and there is no layer thickness variation except at the center fold. Cognizant of the overall scaling of gain/absorption with

#167148 - $15.00 USD Received 20 Apr 2012; revised 7 Jun 2012; accepted 7 Jun 2012; published 26 Jun 2012

$1/v_g$, we have adjusted the gain in each species so that the product of the gain times the index is a constant for each plot. We note the following: (1) Gain enhancement is observed on both band edges, but if the gain medium is in the high refractive index material, the right band edge is enhanced more, consistent with our experimental results shown in Fig. 2; if the gain medium were in the low refractive material, we would expect the left edge to be enhanced more. (2) The gain at the reflection band defect is enhanced more than that at the band edges in either configuration. (3) The greatest gain enhancement is obtained when the folding is against the low refractive index material and the gain medium is also in the low refractive index layers. (We could not realize this case experimentally because the R6G dye was not compatible with the THV polymer during extrusion.) In our experiments, lasing efficiencies were comparable for samples folded in either direction so that we could not conclude that one outperformed the other consistently. This uncertainty is increased because the R6G gain curve is not spectrally flat and layer thickness disorder was not negligible, as compared to our simulated results. The linewidth of the defect peak will affect performance, and we expect that layer thickness variations may further increase the laser linewidth as well as the threshold.

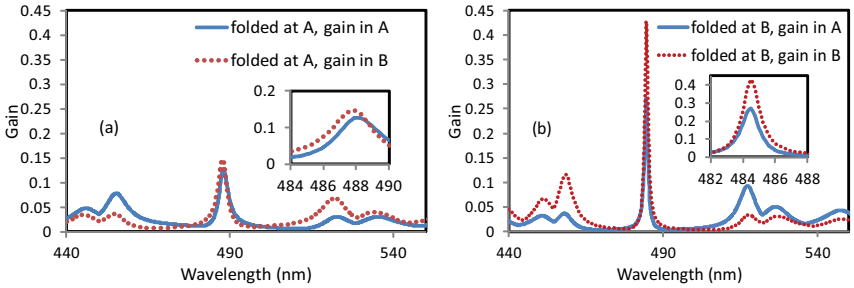

Fig. 5. Gain enhancement in a 128-layer folded DFB laser film. (a) Gain is in the higher refractive index *A* layers and the fold is against an *A* layer (solid blue trace); gain is in the lower index *B* layers and the fold is against an *A* layer (dotted red trace). (b) Gain is in *A* and fold is against *B* (solid blue trace); gain is in *B* and fold is against *B* (dotted red trace).

4. Conclusion

We have shown that the flexibility of stand-alone all-polymer multilayer DFB laser films allows folding to create a thicker center layer. The result of this folding is not only a spectral defect in the reflection band that becomes the preferred lasing wavelength, but also significantly improved efficiency and a lower lasing threshold, as has been seen in other lasing media [11, 23]. Through simulations, we understand that these improvements can be explained by the increased interaction between the optical field and the gain medium. By manipulating the center phase shift by terracing the center layer, we have shown that the location of the reflection band defect can be shifted, leading to post-extrusion tunability for the folded DFB laser, taking advantage of the broad inherent tunability of the dye-doped gain medium.

Acknowledgments

The authors are grateful to the National Science Foundation for financial support from the Science and Technology Center for Layered Polymeric Systems under grant number No. DMR 0423914 and to the State of Ohio, Department of Development, State of Ohio, Chancellor of the Board of Regents and Third Frontier Commission, which provided funding in support of the Research Cluster on Surfaces in Advanced Materials.

#167148 - $15.00 USD Received 20 Apr 2012; revised 7 Jun 2012; accepted 7 Jun 2012; published 26 Jun 2012